Published in final edited form as:

Magn Reson Med. 2019 March ; 81(3): 1964–1978. doi:10.1002/mrm.27548.

Perfusion of the Placenta assessed using Arterial Spin Labeling and Ferumoxytol Dynamic Contrast Enhanced Magnetic Resonance Imaging in the Rhesus Macaque

Kai D. Ludwig[1], **Sean B. Fain**[1,2,3], **Sydney M. Nguyen**[4,5], **Thaddeus G. Golos**[4,5,6], **Scott B. Reeder**[1,2,3,7,8], **Ian M. Bird**[5], **Dinesh M. Shah**[5], **Oliver E. Wieben**[1,2], **Kevin M. Johnson**[1,2,*]

[1]Medical Physics, University of Wisconsin, 1111 Highland Ave, Madison, Madison, WI, USA 53705

[2]Radiology, University of Wisconsin, 600 Highland Ave, Madison, Madison, WI, USA 53792

[3]Biomedical Engineering, University of Wisconsin, 1415 Engineering Dr, Madison, Madison, WI, USA 53706

[4]Wisconsin National Primate Research Center, 1220 Capitol Court, Madison, WI, USA 53715

[5]Obstetrics and Gynecology, University of Wisconsin, 600 Highland Ave, Madison, WI, USA 53792

[6]Comparative Biosciences, University of Wisconsin, 2015 Linden Dr, Madison, Madison, WI, USA 53706

[7]Medicine, University of Wisconsin, 600 Highland Ave, Madison, Madison, WI, USA 53792

[8]Emergency Medicine, University of Wisconsin, 600 Highland Ave, Madison, Madison, WI, USA 53792

Abstract

Purpose: To investigate the correspondence between arterial spin labeling (ASL) flow-sensitive alternating inversion recovery (FAIR) and ferumoxytol dynamic contrast enhanced (DCE) magnetic resonance imaging (MRI) for the assessment of placental intervillous perfusion.

Methods: Ten pregnant macaques in late 2nd trimester were imaged at 3T using a 2D ASL FAIR, with and without outer volume saturation (OVS) pulses used to control the bolus width, and a 3D ferumoxytol DCE MRI acquisition. ASL tagged/control pairs were averaged, subtracted, and normalized to create perfusion ratio maps. Contrast arrival time and uptake slope were estimated by fitting DCE data to a sigmoid function. Macaques (N=4) received interleukin-1β to induce inflammation and disrupt perfusion.

Results: FAIR tag modification with OVS reduced median ASL ratio percentage compared to conventional FAIR (0.64±1.42% vs. 0.71±2.00%;p<0.05). Extended ferumoxytol arrival times (34±25sec) were observed across the placenta. No significant DCE signal change was measured in fetal tissue (−0.6±3.0%;p=0.52) or amniotic fluid (1.9±8.8%;p=0.59). High ASL ratio was

*Correspondence to: Kevin M. Johnson, PhD, 1111 Highland Avenue, Room L1133, Madison, Wisconsin, USA 53705-2275. kmjohnson3@wisc.edu.

significantly correlated with early arrival time and high uptake slope ($p<0.05$) but ASL signal was not above noise in late-DCE-enhancing regions. No significant differences were observed in perfusion measurements between the interleukin-1β and controls ($p>0.05$).

Conclusion: ASL FAIR and ferumoxytol DCE MRI are feasible methods to detect early blood delivery to the macaque placenta. OVS reduced high macrovascular ASL signal. Interleukin-1β exposure did not alter placental intervillous perfusion. An endogenous-labeling perfusion technique is limited due to extended transit times for flow within the placenta beyond the immediate vicinity of the maternal spiral arteries.

Keywords

placenta; magnetic resonance imaging; arterial spin labeling; dynamic contrast enhanced; pregnancy; obstetrics; intervillous perfusion; ferumoxytol; rhesus macaque

INTRODUCTION

The placenta supplies nutrients and oxygen to the fetus while removing waste products and consists of a complex, maternal-fetal interface. Maternal blood is delivered to the placenta via spiral arteries which conduct blood from the maternal arteries to the intervillous space surrounding the placental chorionic villi [1]. Fetal blood circulates separately within the villi that are floating in the maternal blood in the intervillous space or anchored to the maternal decidua. Abnormal placental function can be life threatening and have long-term effects both for maternal and fetal health [2]. For example, deficiencies in perfusion impede the nutrient exchange affecting placental function and fetal development [3]. Potentially in response to the reduced nutrient exchange, 3–7% of first-time mothers develop pre-eclampsia (a hypertensive disorder of pregnancy) [4] and in some cases growth restriction of the fetus may result.

Despite its crucial role in fetal development, the placenta is poorly understood, due in part to the limited non-invasive methods to study the placenta throughout pregnancy [5]. Ultrasound is a primary imaging modality for the assessment of placenta and fetal health due to its low cost, strong safety profile, and real-time image capabilities. Unfortunately, ultrasound provides a limited number of image contrasts and thus may be insensitive in detecting early functional precursors to pregnancy complications.

Magnetic resonance imaging (MRI) is an emerging modality for the longitudinal monitoring of placental health in utero. It has an excellent safety profile and can acquire 3D volumes in any orientation with multiple contrasts including functional measures. Quantitative, non-contrast-enhanced perfusion MRI methods like arterial spin labeling (ASL) are promising approaches for the safe evaluation of placental perfusion [6]. For example, ASL with flow-sensitive alternating inversion recovery (FAIR) acquires images with a global and slice-selective inversion to tag inflowing blood outside a slice of interest resulting in perfusion contrast [7]. The FAIR labeling scheme is effective for assessment of multi-directional flow into the tissue of interest (e.g. placenta) without the need to locate the feeding arteries. Prior work has investigated FAIR in human placentas demonstrating feasibility of the FAIR scheme to quantify placental perfusion in healthy human mothers [8] and detecting low

perfusion in the basal plate of the placenta, a sign that is predictive of “small for gestational age” neonates [6].

Despite the success of initial placenta ASL, perfusion quantification is potentially complicated by the unique maternal vascular network perfusing the placenta that lacks a traditional capillary bed and contains multiple arterial input sources. ASL has contributions from both perfused blood signal that has left the vasculature and from blood signal remaining within the vasculature. To mitigate vascular signal, the timing of ASL tagging must be adapted to the vascular system. In the case of FAIR ASL, saturation pulses can be played out after a specified delay time to allow for a post-label delay as was first introduced in the brain with inferior saturation RF [9, 10]. The post-labeling delay must match the transit time of blood from its tag location to location of perfusion for accurate quantification. Vascular spaces of the intervillous circulation are relatively large, potentially leading to long blood transit times. Long transit times will prohibit ASL analysis in regions since the persistence of the ASL signal transit times relies on the bolus transit times. This is among other confounders including the T_1 time of labeled blood, variation in labeling efficiency, low signal to noise ratio (SNR), and the contributions from fetal circulations.

Dynamic contrast enhanced (DCE) MRI offers an alternative, and potentially more robust, technique to measure maternal placenta perfusion. DCE MRI collects of a series of T_1-weighted images, with high temporal resolution, throughout the injection of a T_1-shortening contrast agent, which enhances local signal [11]. Perfusion can be assessed through tracer kinetic modeling of the signal-time curves in the tissue of interest [12]. DCE has relatively high SNR and has demonstrated agreement with ASL in the measurement of renal blood flow [13] and relative pulmonary blood flow [14]. It is also potentially more robust in slow perfusing organs (e.g. placenta, liver) comparatively with ASL. Gadolinium-based contrast agent (GBCA) DCE MRI in the rhesus macaque has been demonstrated for the estimation of contrast arrival times, and detection of placental spiral artery locations [15, 16]. While GBCA’s have shown efficacy in measuring perfusion, they are known to cross the placenta and are contraindicated in humans due to concerns for teratogenicity and known long-term sequalae of in utero GBCA exposure [17].

Ferumoxytol, an ultra-small superparamagnetic iron oxide nanoparticle (SPION), offers an FDA-approved alternative to GBCA’s. Although approved for intravenous iron supplementation to treat anemia, there is evidence supporting its off-label use as an intravascular agent contrast agent for dynamic susceptibility contrast (DSC) and DCE MRI. Ferumoxytol, being of large molecular size, and due to entrapment by macrophages on the maternal side, is unlikely to cross the placental barrier. Phagocytosis of SPIONs by macrophages allows MRI of SPIONs to be used as a biomarker macrophage infiltration in infection and inflammation [18]. Further, the T_1 shortening properties of ferumoxytol enable both visualization of the vasculature and perfusion measurements in the placental tissue.

Limited studies currently exist that evaluate non-contrast perfusion methods, such as ASL, with reference contrast methods, such as ferumoxytol DCE, specifically in the placenta. The rhesus macaque (*Macaca mulatta*) is a suitable experimental model to develop MR imaging methodologies during gestation with a placental villous organization and number of

offspring similar to humans [19]. The objective of this work is to evaluate the potential of two variants of ASL MRI with FAIR, with and without outer volume saturation (OVS) pulses, to assess placental intervillous perfusion without contrast reagents, then compare with a "gold-standard" reference, ferumoxytol DCE MRI in animals receiving interleukin-1β (IL-1β) and healthy controls. Intra-amniotic fluid injection of IL-1β has previously been shown to induce chorioamnionitis and preterm labor in the rhesus macaque [20, 21]. The induced inflammation response could potentially disrupt perfusion. We hypothesize that acute inflammation may also perturb placental intervillous perfusion, measurable by MRI methods.

METHODS

Animal Population

All procedures were approved by the Institutional Animal Care and Use Committee at the University of Wisconsin-Madison. Ten healthy, pregnant rhesus macaques (*Macaca mulatta*) underwent MRI in the late second trimester (mean±standard deviation (SD)=99.2±5.9 days) based on an average 166-day macaque pregnancy length [22] with an average maternal weight of 8.93±1.03 kg. Table 1 summarizes the characteristics of the animal and treatment groups studied. Animals were divided into three treatment groups: no intervention, saline injection, or IL-1β (human IL-1β, PeproTech, Rocky Hill, NJ, USA) treated. Animals received an intra-amniotic injection of 10 μg of IL-1β in 0.5 mL sterile saline (N=4), 0.5 mL saline (N=3), or no injection (N=3). We performed the IL-1β infusion to induce an inflammation response and promote immune cell trafficking, but that is not the focus of the work presented here.

Imaging Acquisitions

All imaging was performed on a clinical 3.0T MRI system (Discovery MR750, GE Healthcare, Waukesha, WI, USA) with a 32-channel phased array torso coil (Neocoil, Pewaukee, WI). Rhesus macaques were sedated with 1.5% isoflurane supplemented with O_2 using a portable anesthesia system and imaged in a right-lateral position.

Anatomical MRI—A stack of 2D, T_2-weighted anatomical MR images was acquired using a single-shot fast spin echo (SSFSE) data readout with a repetition time (TR)=3.0–4.0 sec, echo time (TE)=100.3 ms, receiver bandwidth (BW)=651 Hz/voxel, matrix=256×128, in-plane spatial resolution=0.70 mm, slice thickness=2.0 mm, with 40–70 slices in both the sagittal and axial orientation with complete coverage of the placenta.

ASL MRI—Pulsed ASL FAIR imaging [7] was performed using a 2D, single-slice, respiratory-triggered acquisition with an SSFSE data readout (TR=5.0–7.0 sec, TE=49.2 ms, BW=651 Hz/voxel, matrix=128×128, field-of-view (FOV)=18×18 cm, in-plane spatial resolution=0.70 mm, readout slice thickness=4 mm, selective inversion slice thickness=14 mm, and 2 dummy scans for a total scan time of ~6 minutes depending on respiratory rate). Images were acquired under free breathing conditions with the 2.0 sec inversion time (TI) chosen such that tagging and imaging occurred at end-expiration resulting in a variable TR between animals. Control and FAIR tagged images were alternated until 40 total images (20

control/tag pairs) were acquired. A proton density weighted image (M_0) was obtained prior to the control/tag pairs using no magnetization preparation. ASL FAIR imaging was performed with and without outer volume saturation (OVS) using RF pulses applied above and below the ASL imaging plane, similar to the QUIPSS II approach [9]. OVS pulses were used to limit the temporal width of the ASL bolus by saturation the late-arriving FAIR-labeled spins. This has the objective of reducing sensitivity to bolus arrival time and minimizing hyper-intense signal from the macrovasculature. OVS pulses were applied 1.0 sec after the inversion preparation using flip=90°, 100 mm superior-to-inferior coverage, and 10 ms quadratic phase RF pulses resulting in a bolus width of TI_1=1.0 sec. The ASL FAIR pulse sequence with OVS pulses added will be denoted, +OVS, and without, -OVS, throughout the manuscript. Fig 1 shows diagrams of the two ASL FAIR pulse sequences and their theoretical ASL signal as a function of transit time.

DCE MRI—DCE was acquired with a 3D T_1-weighted spoiled gradient echo with differential subsampling with Cartesian ordering (DISCO) [23] with 2 point fat/water separation (TR=4.8 ms, TE_1/TE_2,=1.2/2.4 ms, BW=1116 Hz/voxel, matrix=256×128×128, FOV=22×15.4×12.8 cm, spatial resolution=0.86×0.86×1.0 mm, temporal resolution=5 sec, total scan time=200–300 sec, flip=12°, ARC acceleration factor=2×2) throughout injection of 4 mg/kg ferumoxytol (Feraheme™, AMAG Pharmaceuticals, Waltham, MA, USA) diluted 5:1 with saline and infused intravenously over 20 sec allowing for direct measurement of contrast arrival time to placental tissue.

Magnetic Resonance Angiography—High resolution ferumoxytol-enhanced magnetic resonance angiogram (MRA) data were acquired with a respiratory gated 3D, T_1-weighted ultrashort echo time (UTE) acquisition with center-out radial trajectory [24] (TR=4.4 ms, TE=0.13 ms, BW=694 Hz/voxel, matrix=360×360×360, FOV=18×18×18 cm, spatial resolution =0.5×0.5×0.5 mm, flip=10°, scan time=5:33) both pre- and post-injection of ferumoxytol. Volume rendering was performed on the complex subtracted MRA data using Horos DICOM viewer (Horos Project).

Image Analysis

MRI data reconstruction and analysis was performed using custom scripts in MATLAB (MathWorks, Natick, MA) unless otherwise noted. Image segmentation of the placental tissue was performed using the M_0 image. All ASL FAIR tagged/control pair images were co-registered to the M_0 image using MelastiX, a collection of MATLAB wrappers for the image registration suite Elastix [25, 26]. DCE volumetric data were resampled and registered to the ASL slice using the Advanced Normalization Tools (ANTs) [27]. Supporting Information Figure S1 shows the entire image registration pipeline between the DCE and ASL data with step-wise explanations.

ASL data was processed by separately averaging then subtracting the FAIR tagged and control pairs to create an ASL signal difference image (ΔM). ASL ratio maps were created using Eq. 1 below by normalizing ΔM to M_0.

$$ASL\ Ratio\ Map = 100\% \bullet \frac{\Delta M/M_0}{TI_1} \quad [1]$$

For comparisons between ASL FAIR -OVS and +OVS, the ratio maps were divided by the ASL bolus width (TI_1=TI=2 sec in the -OVS case) to account for the FAIR tagged inflow duration.

Conventional ASL analysis in organs with traditional capillary beds (e.g. brain, kidney, etc.) entails fitting the ASL signal to a single-parameter implementation of the general kinetic model [28]. Given the unusual maternal vascular circulation within the intervillous space of the placenta, absolute quantification of ASL data could have substantial errors. We have chosen to represent the ASL signal as an ASL ratio map, in units of percentage. This is a semi-quantitative parameter of the perfusion signal and will be proportional to the blood delivery to the placental intervillous space.

DCE data was analyzed with a semi-quantitative method. The signal intensity (SI) from the DCE data over time (t) was fit to the generalized sigmoid-shaped logistic function (i.e. S-shaped curve with plateau),

$$SI(t) = SI_0 + \left(SI_{max} - SI_0\right)/(1 + \exp(-s(t-d))) \quad [2]$$

on a per voxel basis to determine the contrast delay time (d), a contrast uptake steepness factor (s), the maximum signal intensity (SI_{max}), and baseline signal intensity (SI_0) for every placental voxel. This fitting function choice closely matched the observed ferumoxytol DCE signal-time curves within the placental tissue with no appreciable contrast agent washout. Unlike alternative tracer-kinetic models, this approach is not sensitive to accurate measurement of the arterial input function, which is challenging to estimate in the placenta due to the multiple arterial inputs. The general shape of the sigmoid-shaped function and derivative $\left(\frac{d}{dt}SI(t)\right)$ are shown for simulated data in Supporting Information Figure S2a along with in vivo DCE data, the sigmoid-shaped fit, and estimated parameters in Supporting Information Figure S2b. The contrast delay times were shifted relative to the injection time to derive the contrast arrival time (i.e. delay time from contrast injection to 50% maximum enhancement). The relative blood flow (rBF) was estimated to be equivalent to the slope of the contrast uptake curve.

To determine the fetal change in SI (ΔSI) from the ferumoxytol contrast, ROIs were manually drawn on a single slice containing both fetal tissue and amniotic fluid. The percent ΔSI was calculated using Eq. 3 below

$$\Delta SI = 100\% \bullet \left(SI_f - SI_i\right)/SI_i \quad [3]$$

using the SI from the initial (SI_i) and final (SI_f) time frame in the DCE data.

Statistical Analysis

A Wilcoxon rank-sum test was performed between the distributions of the ASL FAIR ratio percentages within the placenta using either +OVS or –OVS tag modifications by combining data from all animals. A Wilcoxon rank-sum test was performed between the grouped ASL FAIR +OVS ratio percentage and DCE arrival times as well as the grouped ASL FAIR +OVS ratio percentage and DCE uptake slope. To determine a significant change in the DCE signal intensity, a paired, two-sided Student t-test was performed between SI_i and SI_f averaged across all animals. Statistical significance was defined as a p-value<0.05.

RESULTS

The 3D volume renderings of the MRA, shown in Fig. 2a demonstrate the highly vascular nature of the rhesus placenta in the uterine space, and the ability of ferumoxytol enhanced MRA to visualize the placental vasculature. Maternal blood supply to the placenta and growing fetus, originates in the uterine arteries prior to delivery to the placenta through the radial and spiral arteries. The major feeding arteries and draining veins are highlighted. The rhesus macaque placenta is typically bi-lobed (i.e., two separate placental discs, with the primary disc having the insertion of the umbilical cord, and connected to the secondary disc by several arteries and veins) and differs from typical single lobed human placental anatomy in this respect. Fig. 2b shows T_2-weighted anatomical MR images of the macaque placenta with the placental tissue separately outlined. Several other anatomical features are highlighted to orient the reader.

Fig. 3a (top row) shows the averaged FAIR tagged, control, and ASL perfusion ratio map (color) overlaid on the M_0 image (gray) from the ASL FAIR –OVS acquisition. The ratio map shows focal signal enhancements within the placenta and in its surrounding vasculature. Fig. 3a (bottom row) shows the ratio map from the +OVS acquisition depicting similar localized regions of high perfusion with predominately noise elsewhere. A histogram distribution of the ratio percentages within the placenta for the two FAIR acquisitions is displayed in Fig. 3b showing a reduction in the median ratio percentage and saturation of high ASL ratio voxels (>10%). The ASL ratios for both FAIR acquisitions in each of the ten individual macaques and all animals grouped together are shown as box-and-whisker plots in Fig. 4a. Fig. 4b shows a voxel-wise density plot of the ASL ratio between the two FAIR variants with voxels having reduced ASL ratio with addition of OVS pulses circled. OVS pulses significantly (p<0.05) reduced the median ASL ratio (+OVS=0.64±1.42%) compared to without OVS pules (–OVS=0.71±2.00%). Table 2 summarizes the placental perfusion values (median±SD and quartile values (5%−95%)) of the ASL ratio for all interventions.

Heterogeneous contrast arrival times and localized regions of contrast in-flow are observable in the volumetric maximum-intensity projections (MIPs) (Fig. 5a) and single slice DCE MRI series (Fig. 5b) of corresponding time-frames. The DCE signal enhancement curve and fits for voxels representing ‘early-enhancing’ and ‘late-enhancing’ placental regions or fetal regions are shown in Fig. 5c. Differences in enhancement time within placental regions is approximately 10’s of seconds. From the sigmoid-shaped fits, contrast arrival time (Fig. 5d) and relative blood flow (uptake curve slope) maps (Fig. 5e) are derived. Table 3 summarizes the ferumoxytol DCE measurements for all interventions. The median contrast arrival time

from the time of injection for all cases was 34±25 sec and ranged from 14–87 sec (5–95% quartile) with a median relative blood flow of 102±39 sec^{-1}.

No ferumoxytol signal enhancement was observable within the fetus or amniotic fluid. The percent change in the signal intensity was calculated for both from the 4D DCE data. A non-significant relative signal change was measured to be −0.6±3.0% for fetal tissue (p=0.52) and 1.9±8.8% for the amniotic fluid (p=0.59) across all animals in the study.

A regional comparison for one case in Fig. 6 shows the parametric maps of perfusion: ASL (FAIR +OVS) ratio (a), DCE contrast arrival times (b), and DCE relative blood flow (c) within the placental tissue. Spatial similarities can be observed between voxels exhibiting high ASL ratio, early contrast arrival, and high relative blood flow. Locations within placental tissue that display long contrast arrival times also show low ASL ratio percentage which are likely dominated by noise (<0.5% ASL ratio). These trends can be observed in the voxel-wise density plots of ASL ratio and contrast arrival times (Fig. 6d) and between ASL ratio and uptake slope (Fig. 6e) in the placental tissue for the single case. The circled region in Fig. 6d shows many voxels with high ASL ratio having short contrast arrival times while voxels with long contrast arrival times tended to have very low ASL ratio. The highlighted region in Fig. 6e showed a slight association between voxels with high ASL ratio coinciding with voxels with high uptake slope.

The voxels with early contrast arrival were significantly (p<<0.05) correlated with voxels with high ASL ratio percentage, which can be seen in the box-and-whiskers plots (Fig. 7a). Fig. 7b shows a voxel-wise density plot for all placental voxels across the entire group of monkeys studied demonstrating a large frequency of voxels with early DCE arrival time and high ASL signal. Further, Fig. 7c shows a box-and-whiskers plot where voxels with high uptake slope were also significantly (p<<0.05) correlated with voxels with high ASL ratio percentage. The voxel-wise density plot for all voxels and all animals is shown in Fig. 7d.

DISCUSSION

In this work, ASL FAIR and ferumoxytol DCE MRI were shown to be feasible to detect early blood delivery to the placenta in a pregnant rhesus macaque model. Regions of intense ASL perfusion signal were correlated spatially to early arrival times and increased slope of contrast agent uptake on DCE MRI. Likely, both ASL FAIR and ferumoxytol DCE MRI can identify the locations of the maternal decidual spiral arteries entering the placental intervillous space. We performed IL-1β infusions to induce inflammation and potentially disrupt perfusion. However, no statistically significant differences were observed between the IL-1β injected group and the control groups in the ASL ratio or DCE contrast arrival time and relative blood flow. Sub-analysis of the groups should be considered preliminary due to low numbers.

The heterogeneous nature of intervillous perfusion signal in ASL FAIR suggests that a voxel-wise interpretation at distal regions from the spiral arteries may be confounded by the limits of the FAIR inversion tagging duration and delay. This observation is corroborated by the extended transit time across the placental region from ferumoxytol DCE images. While

some of this variation may be compensated in ASL by labeling closer to placental regions and with a tighter bolus to limit dispersion, these adaptations will not address the extended transit times. Thus, the unique intervillous space of the placenta that leads to extended transit times is likely the reason for the low correlation between ASL and DCE observed in our study. In ASL FAIR, and ASL generally, for any signal difference to occur, spins must travel from the labeling region to the imaging voxel within a post-label delay period. In this work, this delay was 2.0 sec, a typical value used for ASL at 3.0T. Extending the post-label delay would theoretically allow for ASL with reduced transit time dependence but with the tradeoff that the magnetic-inversion label will decay exponentially according to the T_1 of blood (T_1=~1.6 sec at 3T [29]) degrading SNR.

The contrast arrival times and relative blood flow were estimated using a simplified, semi-quantitative approach based on the empirical uptake curves behaving in a sigmoidal fashion since limited literature exists for absolute quantification of ferumoxytol DCE MRI data. Most animals showed similar regions of high ASL ratios, early contrast arrival time, and higher uptake slope. Blood delivery through the spiral arteries should have the highest velocity and slow down upon entering the intervillous space. In some animals, regions with high ASL ratio and early arrival time are adjacent to regions with higher uptake slope. Additionally, some regions with high uptake slope do not coincide with regions having early contrast arrival time or high ASL signal. This may be physiological with more complex flow patterns within the intervillous space being measured such as a narrow portion of the placental tissue where ferumoxytol contrast quickly fills. Regions with high ASL signal and long contrast arrival times may be potentially from fetal perfusion. ASL FAIR analysis ignores contributions from fetal circulations and may overestimate placental perfusion as a result. The distribution of DCE arrival times within the placenta were substantially longer than the 2.0 sec ASL TI. In distal portions of the placenta with late enhancment, the contrast arrival times are upwards of 70 seconds from the injection time to completely fill. The contrast arrival is much faster in early enhancing regions. These times preclude measurement by spatially-based ASL methods due to loss of ASL label. The early contrast arrival portions may be able to predict the locations of ASL and vice versa but distal portions with slow uptake, noise predominates the ASL ratio images. The ASL data is likely uninformative beyond the immediate vicinity of the spiral arteries.

Additional saturation RF pulses (e.g. QUIPSS II and Q2TIPS) have previously been shown to minimize systematic error caused by variable transit time of labeled blood and remove contaminating macro-vascular signal for brain applications [9, 10]. Here, we have applied saturation pulses to the tagging region above and below the imaging slice to limit the ASL bolus width. A controlled ASL bolus width is recommended for quantification, allowing transport of the tagged magnetization into the extravascular space and to avoid intravascular signal. In the case of the placenta, blood is delivered to the tissue via spiral arteries after which it enters the intervillous space, a blood compartment. There the magnetization is subject to motion within the intervillous space, and exchange with the placenta tissue and fetal circulation. With our ASL timing, using OVS would allow for measurements insensitive to a 1s difference in the bolus arrival time. This is significantly less that the heterogeneity observed in DCE. Thus, the major affect of the OVS was to suppress the macro-vasculature signal, particularly on the periphery of the placenta. A fraction of the

observed ASL signal is still intravascular residing in the intervillous space. OVS did additionally lower the median ASL signal, which is expected due to the shorter bolus width, a reduction of partial volume artifacts from large vessels, and off-resonance magnetization transfer.

The endogenous, non-invasive nature of ASL is advantageous for safety and cost reasons when translating to human patients. While placental ASL perfusion has been investigated in humans [6, 8, 30], animal studies with reference standards are limited. Currently, no ASL perfusion studies exist in the rhesus macaque placenta for which to compare these results. In humans however, ASL FAIR has been shown to be sensitive to detect a greater proportion of low perfusion voxels in intrauterine growth restricted patients versus controls [8, 30] and reduced perfusion in the basal region of the placenta in mothers who delivered small for gestational age neonates [6]. Given the comparisons in this study and these results, it is conceivable that the distribution of early arriving blood is sufficient to determine the overall health of the placenta. Spatially-based ASL methods may still prove valuable in measuring blood flow to the intervillous space near the vicinity of spiral arteries. Spiral artery remodeling during pregnancy is essential to maximize the delivery of maternal blood to the intervillous space at suitably low velocity [31]. Maladaptation of the spiral arteries has been associated with several gestational complications including pre-eclampsia and intrauterine growth restriction [32, 33]. However, in defining the pathogenesis, the ASL signal may not fully represent the perfusion signal.

FAIR ASL does have limitations with respect to imaging the placenta. In FAIR, the labeling plane and imaging plane are identical. Thus, there is potential for the imaging slab to intersect with the feeding arteries and potential for tagging of venous, fetal, and intervillous flow. An axial/transverse slab was chosen in this work. This puts the ASL plane roughly orthogonal to the feeding uterine arteries but may intersect with in-plane spiral arteries. Alternative ASL variants have been explored to measure placental perfusion in humans including pseudo-continuous ASL (pCASL) [34] and velocity-selective ASL (VSASL) [35, 36]. pCASL utilizes a train of short RF pulses to invert the magnetization of blood as it flows through a thin labeling plane. Recent work applying pCASL in the human placenta at 3T [37] shows localized perfused regions with high signal intensity, similar to the results presented here. pCASL showed promise to estimate the placental blood flow and arterial transit time in healthy subjects imaged in the second trimester. While pCASL shows higher SNR than pulsed ASL methods (e.g. FAIR), the labeling technique suffers from extended arterial blood delay times between the labeling and imaging location (i.e. placenta). Furthermore, the feeding arteries must be located to place the labeling plane, which is difficult for the placenta.

The extended arrival time across the placental region from ferumoxytol DCE MRI, median=34 sec from the injection time, are qualitatively similar to that observed by others using GBCA’s in the rhesus macaque [15, 38] and iron in mice [39]. Though not specifically reported on a voxel-wise basis, the contrast arrival times to the placenta appear to be approximately 10’s of sec, with distant portions taking upwards of 1 min. In humans, Burchell demonstrated 2–3 sec arrival times of contrast dye into the intervillous space after injected through an aorta catheter [40] measure by X-ray. Diffusion of the dye took roughly

30 sec in late-gestational stage women with the diffusion rate depending on the spiral artery and location within the placenta. Similarly, Borell et al. quoted “first seen” dye contrast into the intervillous space in humans of 3–11 sec and qualitatively described slow filling at more distal portions of the placenta [41]. The longer arrival times reported in this study are likely due to the 20 sec venous infusion resulting in contrast dispersion. Additionally, arrival time was calculated at the 50% enhancement hence, slow enhancement would lead to extended estimates of the contrast arrival.

We have shown non-significant enhancement of the fetal tissue and amniotic fluid throughout the DCE acquisition providing evidence that ferumoxytol is not immediately taken up into these tissues. MRI contrast agents, primarily GBCA, have previously been used to enhance placental visualization and identify maternal decidual spiral arteries in humans [42], the rhesus macaque [15, 16, 38, 43, 44] and a variety of small animal models [45–50]. However, most GBCA’s exchange with the extravascular space. Recently, GBCA’s were shown to be at nearly undetectable levels in the fetal and placental tissue in non-human primates [51] after intravenous infusion for DCE MRI, but they have previously been observed in the bladder of the fetus [38]. Ferumoxytol can be administered during pregnancy similar to other intravenous iron preparations but is safer and produces fewer allergic and idiosyncratic reactions [52]. Pregnancy is a physiological iron-deficient state and as such presents an imaging opportunity with efficient iron delivery by ferumoxytol without risk of iron overload [53]. Further, its long intravascular half-life (~14–15 hrs.) compared to GBCA makes ferumoxytol a useful agent for consideration as a vascular MRI T_1 shortening contrast agent.

MRI techniques to measure tissue perfusion based on motion rather than spatial-labeling of blood exist such as, previously mentioned, VSASL, and intravoxel incoherent motion (IVIM). VSASL tags blood based on flow velocity using flow-sensitizing gradients [35, 36]. VSASL is insensitive to the large transit delays observed in the placenta as has been recently demonstrated [54, 55] and allows for 3D imaging coverage. VSASL demonstrated greater global placental perfusion with differences in regional variation in pregnancies with fetal congenital heart disease compared to controls suggesting VSASL may provide viable biomarkers in early pregnancy detection of dysfunction [55]. IVIM relies on collecting diffusion-weighted MR images with varying degrees of weighting followed by signal modeling of the fast (perfusion) and slow (diffusion) components of water. This technique assumes blood motion is incoherent over a voxel and of higher degree than surrounding tissue [56]. IVIM has been applied to placenta imaging in healthy subjects [57] and demonstrated promise in detecting differences in the perfusion fraction in pregnancies with fetal growth restriction [58], small for gestational age fetuses [59], and in early and late preeclampsia [60] compared to controls. In initial comparisons of placental perfusion, IVIM demonstrated a higher predictive power to reduced birthweight than ASL FAIR [6]. VSASL or IVIM may be better alternatives to ASL FAIR due to reduced dependence on the long transit time. However, strategies for the mitigation of maternal and fetal motion are crucial for motion-based perfusion techniques since encoding of bulk-motion will confound interpretation of the measured signals.

Bulk-motion can also be problematic for pulsed ASL (e.g. FAIR) and DCE MRI acquisitions confounding resulting and/or creating image artifacts, however, IVIM and VSASL are sensitive to much lower levels of motion. In this study, maternal respiratory motion was considered the potentially primary source of bulk motion. Due to anesthesia, negligible fetal motion was qualitatively observed throughout the duration of the ASL and DCE acquisition. The DCE acquisition used a respiratory-gated, acquisition known as DISCO [23] that reconstructs images using pseudo-randomly acquired segmented portions of k-space. The pseudorandom sampling, similar to radial, reduces motion blurring and other motion-related artifacts. These effects are likely small though given the regularity of maternal breathing under anesthesia and were not observable in image. A 2.0 sec TI was chosen to coincide with the maternal respiratory rate ensuring the labeling and imaging region were in an identical respiratory phase and physical location. Furthermore, image registration was performed to mitigate remaining maternal motion. More advanced motion management techniques, reviewed elsewhere [61], may be needed in clinical settings where anesthesia is not commonly used and fetal motion is potentially more significant.

There are several limitations to the current study. The ASL FAIR data represents a single slice acquisition where volumetric coverage of the placenta would be desirable. With dispersion and bolus delays from multiple inputs into the placenta, (i.e. uterine arteries), we have limited the ASL FAIR approach to a single delay time. Thus, a limited representation of entire placental perfusion is shown. Long acquisition times may have contributed to through-plane placental tissue movement between the ASL and DCE acquisitions. Therefore, errors in the volume-to-slice registration of placental tissue may have result in spatial differences between the ASL signal, contrast arrival time, and relative blood flow. Our DCE-fitting algorithm with a sigmoid-shaped function may overestimate contrast arrival times in locations with ‘jets’ of blood. These unusual flow patterns, such as Borell’s jets first demonstrated by MRI using a GBCA [38], would lead to partial enhancements such that the uptake curve would not be sigmoid-shaped, and the contrast arrival time may be overestimated as a result. Perfusion variations may also manifest from different arterial pressures, cardiac outputs, gestational ages as well as positioning.

In conclusion, +OVS reduced the highest ASL FAIR ratio signal compared to -OVS when controlling for labeling duration. ASL FAIR and ferumoxytol DCE MRI are feasible to detect regions of early blood delivery in the placenta in a pregnant rhesus macaque model. In this small, preliminary study, placental intervillous perfusion, as measured by ASL and DCE, was not altered by the IL-1β exposure compared to controls. An endogenous labeling perfusion technique is potentially advantageous when translating to human mothers but is possibly limited due to the extended transit times for placental tissues beyond the immediate vicinity of the maternal spiral arteries.

Supplementary Material

Refer to Web version on PubMed Central for supplementary material.

ACKNOWLEDGMENTS

The authors thank our collaborators and colleagues. We gratefully acknowledge the University of Wisconsin-Madison School of Medicine and Public Health and Departments of Medical Physics, Radiology, and Obstetrics and Gynecology for research support and AMAG Pharmaceuticals, Inc. Waltham, MA for the generous gift of ferumoxytol. In addition, the authors wish to acknowledge support from GE Healthcare who provides research support to UW-Madison. Further, Dr. Reeder is a Romnes Faculty Fellow, and has received an award provided by the University of Wisconsin-Madison Office of the Vice Chancellor for Research and Graduate Education with funding from the Wisconsin Alumni Research Foundation.

Grant sponsor: National Institutes for Health (NIH) Human Placental Project (HPP); Grant numbers: NICHD U01HD087216; Grant sponsor: University of Wisconsin Institute for Clinical and Translation Research (UW ICTR); Grant numbers: UL1 TR000427, TL1 TR000429, Grant sponsor: NIH; Grant numbers: T32 CA009206, K24 DK102595, P51 OD011106; Grant sponsor: Grant sponsor: GE Healthcare; Grant sponsor: University of Wisconsin School of Medicine and Public Health; Grant sponsor: University of Wisconsin Departments of Medical Physics, Radiology, and Obstetrics and Gynecology.

REFERENCES

1. Zaidi SF, et al., Comprehensive Imaging Review of Abnormalities of the Placenta. Ultrasound Q, 2016 32(1): p. 25–42. [PubMed: 26938032]
2. Gandhi S, Ohliger M, and Poder L, State-of-the-Art Imaging of the Placenta. Current Radiology Reports, 2015 3(12): p. 1–13.
3. Krishna U and Bhalerao S, Placental Insufficiency and Fetal Growth Restriction. Journal of Obstetrics and Gynaecology of India, 2011 61(5): p. 505–511. [PubMed: 23024517]
4. Uzan J, et al., Pre-eclampsia: pathophysiology, diagnosis, and management. Vascular Health and Risk Management, 2011 7: p. 467–474. [PubMed: 21822394]
5. Guttmacher AE, Maddox YT, and Spong CY, The Human Placenta Project: placental structure, development, and function in real time. Placenta, 2014 35(5): p. 303–4. [PubMed: 24661567]
6. Derwig I, et al., Association of placental perfusion, as assessed by magnetic resonance imaging and uterine artery Doppler ultrasound, and its relationship to pregnancy outcome. Placenta, 2013 34(10): p. 885–91. [PubMed: 23937958]
7. Kim S-G, Quantification of relative cerebral blood flow change by flow-sensitive alternating inversion recovery (FAIR) technique: Application to functional mapping. Magnetic Resonance in Medicine, 1995 34(3): p. 293–301. [PubMed: 7500865]
8. Gowland PA, et al., In vivo perfusion measurements in the human placenta using echo planar imaging at 0.5 T. Magnetic Resonance in Medicine, 1998 40(3): p. 467–473. [PubMed: 9727951]
9. Wong EC, Buxton RB, and Frank LR, Quantitative imaging of perfusion using a single subtraction (QUIPSS and QUIPSS II). Magn Reson Med, 1998 39(5): p. 702–8. [PubMed: 9581600]
10. Luh WM, et al., QUIPSS II with thin-slice TI1 periodic saturation: a method for improving accuracy of quantitative perfusion imaging using pulsed arterial spin labeling. Magn Reson Med, 1999 41(6): p. 1246–54. [PubMed: 10371458]
11. Khalifa F, et al., Models and methods for analyzing DCE-MRI: A review. Medical Physics, 2014 41(12): p. 124301. [PubMed: 25471985]
12. Sourbron SP and Buckley DL, Classic models for dynamic contrast-enhanced MRI. NMR Biomed, 2013 26(8): p. 1004–27. [PubMed: 23674304]
13. Cutajar M, et al., Comparison of ASL and DCE MRI for the non-invasive measurement of renal blood flow: quantification and reproducibility. European Radiology, 2014 24(6): p. 1300–8. [PubMed: 24599625]
14. Lin YR, et al., Comparison of arterial spin labeling and first-pass dynamic contrast-enhanced MR imaging in the assessment of pulmonary perfusion in humans: the inflow spin-tracer saturation effect. Magn Reson Med, 2004 52(6): p. 1291–301. [PubMed: 15562497]
15. Frias AE, et al., Using dynamic contrast-enhanced MRI to quantitatively characterize maternal vascular organization in the primate placenta. Magn Reson Med, 2015 73(4): p. 1570–8. [PubMed: 24753177]

16. Schabel MC, et al., Functional imaging of the nonhuman primate Placenta with endogenous blood oxygen level–dependent contrast. Magnetic Resonance in Medicine, 2015: p. n/a–n/a.
17. Ray JG, et al., Association Between MRI Exposure During Pregnancy and Fetal and Childhood Outcomes. Jama, 2016 316(9): p. 952–61. [PubMed: 27599330]
18. Neuwelt A, et al., Iron-Based Superparamagnetic Nanoparticle Contrast Agents for MRI of Infection and Inflammation. American Journal of Roentgenology, 2015 204(3): p. W302–W313. [PubMed: 25714316]
19. Golos TG, et al., On the role of placental Major Histocompatibility Complex and decidual leukocytes in implantation and pregnancy success using non-human primate models. Int J Dev Biol, 2010 54(2–3): p. 431–43. [PubMed: 19876826]
20. Presicce P, et al., Neutrophil Recruitment and Activation in Decidua with Intra-Amniotic IL-1beta in the Preterm Rhesus Macaque. Biology of Reproduction, 2015 92(2): p. 56. [PubMed: 25537373]
21. Sadowsky DW, et al., Preterm labor is induced by intraamniotic infusions of interleukin-1beta and tumor necrosis factor-alpha but not by interleukin-6 or interleukin-8 in a nonhuman primate model. Am J Obstet Gynecol, 2006 195(6): p. 1578–89. [PubMed: 17132473]
22. Silk J, et al., Gestation length in rhesus macaques (Macaca mulatta). International Journal of Primatology, 1993 14(1): p. 95–104.
23. Saranathan M, et al., DIfferential Subsampling with Cartesian Ordering (DISCO): a high spatio-temporal resolution Dixon imaging sequence for multiphasic contrast enhanced abdominal imaging. J Magn Reson Imaging, 2012 35(6): p. 1484–92. [PubMed: 22334505]
24. Johnson KM, et al., Optimized 3D ultrashort echo time pulmonary MRI. Magnetic Resonance in Medicine, 2013 70(5): p. 1241–1250. [PubMed: 23213020]
25. Klein S, et al., elastix: A Toolbox for Intensity-Based Medical Image Registration. IEEE Transactions on Medical Imaging, 2010 29(1): p. 196–205. [PubMed: 19923044]
26. Shamonin D, et al., Fast Parallel Image Registration on CPU and GPU for Diagnostic Classification of Alzheimer's Disease. Frontiers in Neuroinformatics, 2014 7(50).
27. Avants BB, et al., A reproducible evaluation of ANTs similarity metric performance in brain image registration. Neuroimage, 2011 54(3): p. 2033–44. [PubMed: 20851191]
28. Buxton RB, et al., A general kinetic model for quantitative perfusion imaging with arterial spin labeling. Magnetic Resonance in Medicine, 1998 40(3): p. 383–396. [PubMed: 9727941]
29. Ingram E, et al., R1 changes in the human placenta at 3 T in response to a maternal oxygen challenge protocol. Placenta, 2016 39: p. 151–3. [PubMed: 26992688]
30. Francis ST, et al., Non-invasive mapping of placental perfusion. Lancet, 1998 351(9113): p. 1397–9. [PubMed: 9593410]
31. Espinoza J, et al., Normal and abnormal transformation of the spiral arteries during pregnancy. J Perinat Med, 2006 34(6): p. 447–58. [PubMed: 17140293]
32. Olofsson P, Laurini RN, and Marsal K, A high uterine artery pulsatility index reflects a defective development of placental bed spiral arteries in pregnancies complicated by hypertension and fetal growth retardation. Eur J Obstet Gynecol Reprod Biol, 1993 49(3): p. 161–8. [PubMed: 8405630]
33. Aardema MW, et al., Uterine artery Doppler flow and uteroplacental vascular pathology in normal pregnancies and pregnancies complicated by pre-eclampsia and small for gestational age fetuses. Placenta, 2001 22(5): p. 405–11. [PubMed: 11373150]
34. Dai W, et al., Continuous flow-driven inversion for arterial spin labeling using pulsed radio frequency and gradient fields. Magn Reson Med, 2008 60(6): p. 1488–97. [PubMed: 19025913]
35. Duhamel G, de Bazelaire C, and Alsop DC, Evaluation of systematic quantification errors in velocity-selective arterial spin labeling of the brain. Magn Reson Med, 2003 50(1): p. 145–53. [PubMed: 12815689]
36. Wong EC, et al., Velocity-selective arterial spin labeling. Magnetic Resonance in Medicine, 2006 55(6): p. 1334–1341. [PubMed: 16700025]
37. Shao X, et al., Measuring human placental blood flow with multidelay 3D GRASE pseudocontinuous arterial spin labeling at 3T. J Magn Reson Imaging, 2018 47(6): p. 1667–1676. [PubMed: 29135072]

38. Panigel M, Wolf G, and Zeleznick A, Magnetic resonance imaging of the placenta in rhesus monkeys, Macaca mulatta. J Med Primatol, 1988 17(1): p. 3–18. [PubMed: 3367357]
39. Deloison B, et al., SPIO-enhanced magnetic resonance imaging study of placental perfusion in a rat model of intrauterine growth restriction. BJOG: An International Journal of Obstetrics & Gynaecology, 2012 119(5): p. 626–633. [PubMed: 22260352]
40. Burchell RC, Arterial blood flow into the human intervillous space. Am J Obstet Gynecol, 1967 98(3): p. 303–11. [PubMed: 5621448]
41. Borell U, et al., Influence of Uterine Contractions on the Uteroplacental Blood Flow at Term. Am J Obstet Gynecol, 1965 93: p. 44–57. [PubMed: 14329169]
42. Marcos HB, Semelka RC, and Worawattanakul S, Normal placenta: gadolinium-enhanced dynamic MR imaging. Radiology, 1997 205(2): p. 493–6. [PubMed: 9356634]
43. Lo JO, et al., Novel Detection of Placental Insufficiency by Magnetic Resonance Imaging in the Nonhuman Primate. Reprod Sci, 2017: p. 1933719117699704.
44. Panigel M, et al., Fast scan magnetic resonance imaging and Doppler ultrasonography of uteroplacental hemodynamics in the rhesus monkey (Macaca mulatta). J Med Primatol, 1993 22(7–8): p. 393–9. [PubMed: 8169942]
45. Taillieu F, et al., Placental perfusion and permeability: simultaneous assessment with dual-echo contrast-enhanced MR imaging in mice. Radiology, 2006 241(3): p. 737–45. [PubMed: 17065560]
46. Yadav BK, et al., A longitudinal study of placental perfusion using dynamic contrast enhanced magnetic resonance imaging in murine pregnancy. Placenta, 2016 43: p. 90–97. [PubMed: 26947613]
47. Shetty AN, et al., A liposomal Gd contrast agent does not cross the mouse placental barrier. Scientific Reports, 2016 6: p. 27863. [PubMed: 27298076]
48. Ghaghada KB, et al., Pre-clinical evaluation of a nanoparticle-based blood-pool contrast agent for MR imaging of the placenta. Placenta, 2017 57: p. 60–70. [PubMed: 28864020]
49. Tomlinson TM, et al., Magnetic resonance imaging of hypoxic injury to the murine placenta. Am J Physiol Regul Integr Comp Physiol, 2010 298(2): p. R312–9. [PubMed: 19923363]
50. Alison M, et al., Measurement of placental perfusion by dynamic contrast-enhanced MRI at 4.7 T. Invest Radiol, 2013 48(7): p. 535–42. [PubMed: 23462675]
51. Prola-Netto J, et al., Gadolinium Chelate Safety in Pregnancy: Barely Detectable Gadolinium Levels in the Juvenile Nonhuman Primate after in Utero Exposure. Radiology, 2017: p. 162534.
52. Avni T, et al., The safety of intravenous iron preparations: systematic review and meta-analysis. Mayo Clin Proc, 2015 90(1): p. 12–23. [PubMed: 25572192]
53. MC M, et al., Williams Obstetrics. 20th Edition ed, ed. C. F 1997: Appleton and Lange.
54. Zun Z, et al., Three-Dimensional Placental Perfusion Imaging Using Velocity-Selective Arterial Spin Labeling. In Proceedings of the 24th Annual Meeting of ISMRM, Singapore, Singapore, 2016: p. 0974.
55. Zun Z, et al., Non-Invasive Placental Perfusion Imaging in Pregnancies Complicated by Fetal Heart Disease Using Velocity-Selective Arterial Spin Labeled MRI. Sci Rep, 2017 7(1): p. 16126. [PubMed: 29170468]
56. Le Bihan D, et al., Separation of diffusion and perfusion in intravoxel incoherent motion MR imaging. Radiology, 1988 168(2): p. 497–505. [PubMed: 3393671]
57. Capuani S, et al., Diffusion and perfusion quantified by Magnetic Resonance Imaging are markers of human placenta development in normal pregnancy. Placenta, 2017 58: p. 33–39. [PubMed: 28962693]
58. Sohlberg S, et al., Magnetic resonance imaging-estimated placental perfusion in fetal growth assessment. Ultrasound Obstet Gynecol, 2015 46(6): p. 700–5. [PubMed: 25640054]
59. Siauve N, et al., Assessment of human placental perfusion by intravoxel incoherent motion MR imaging. J Matern Fetal Neonatal Med, 2017: p. 1–8.
60. Sohlberg S, et al., Placental perfusion in normal pregnancy and early and late preeclampsia: A magnetic resonance imaging study. Placenta, 2014 35(3): p. 202–206. [PubMed: 24529946]
61. Malamateniou C, et al., Motion-Compensation Techniques in Neonatal and Fetal MR Imaging. American Journal of Neuroradiology, 2013 34(6): p. 1124–1136. [PubMed: 22576885]

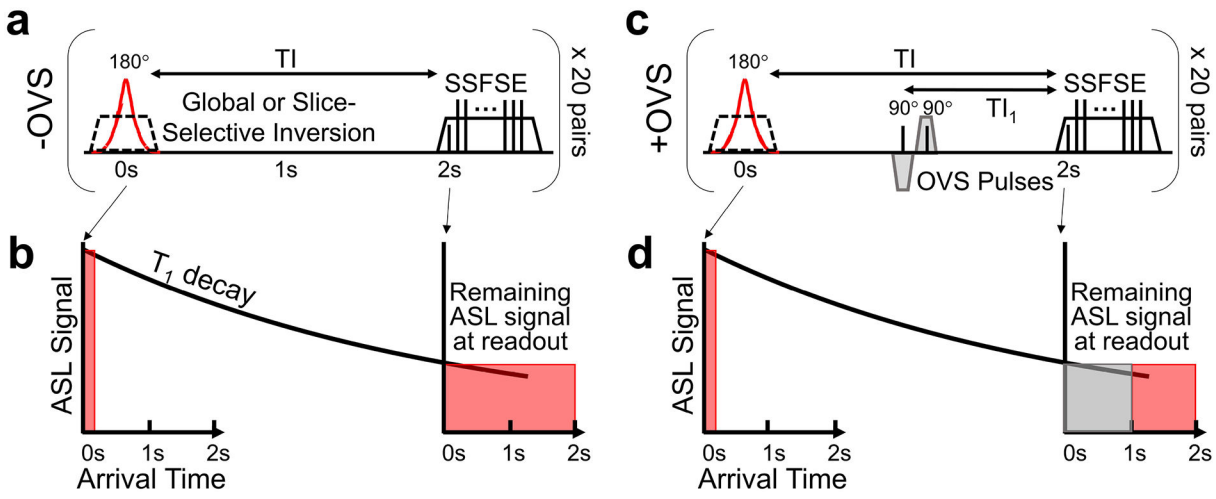

FIG. 1.

Simplified MRI pulse sequence diagrams are shown for both the ASL FAIR acquisitions without (**a**, -OVS) and with (**c**, +OVS) outer volume saturation (OVS) RF pulses. Inverted or FAIR labeled spins are represented by the red color while saturated spins are represented by the gray color. The theoretical ASL signal is shown for the –OVS (**b**) and +OVS (**d**) cases as a function of the blood spins arrival time from labeling region to the placental tissue at two time points during the pulse sequence: immediately after inversion (0 sec) and at imaging readout (TI = 2.0 sec). The remaining ASL signal is governed by assuming a T_1 decay of labeled blood and constant blood flow from the labeling region into the imaging slice. The OVS pulses serve to saturate macrovascular signal in the imaging region and this is depicted as removing the ASL signal with the +OVS schematic.

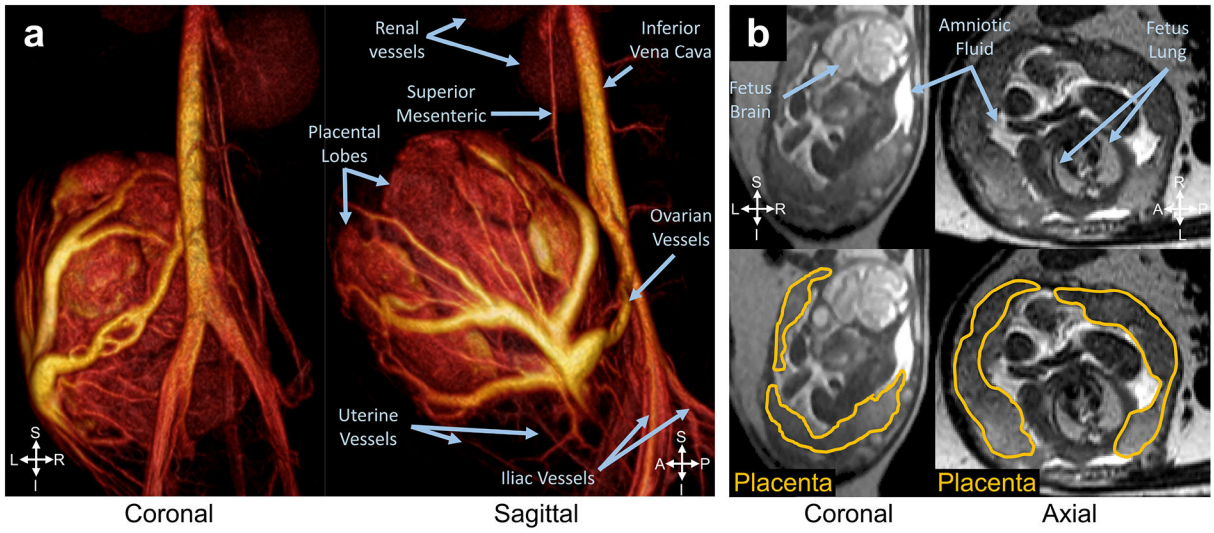

FIG. 2.

Coronal and sagittal views (**a**) of a volume rendered 3D MR ferumoxytol angiogram (MRA) of the rhesus placenta and major blood vessels. The rhesus placenta is a bi-lobular system with blood being supplied from both the left and right uterine and ovarian arteries. Draining vessels are primarily observable in the 3D MRA. Coronal and axial views (**b**), top and bottom row) of an anatomical 2D multi-slice T_2-weighted MR image with the primary and secondary placental lobes outlined. The fetus and bright amniotic fluid are readily observable between the placental lobes in the T_2-weighted anatomical images.

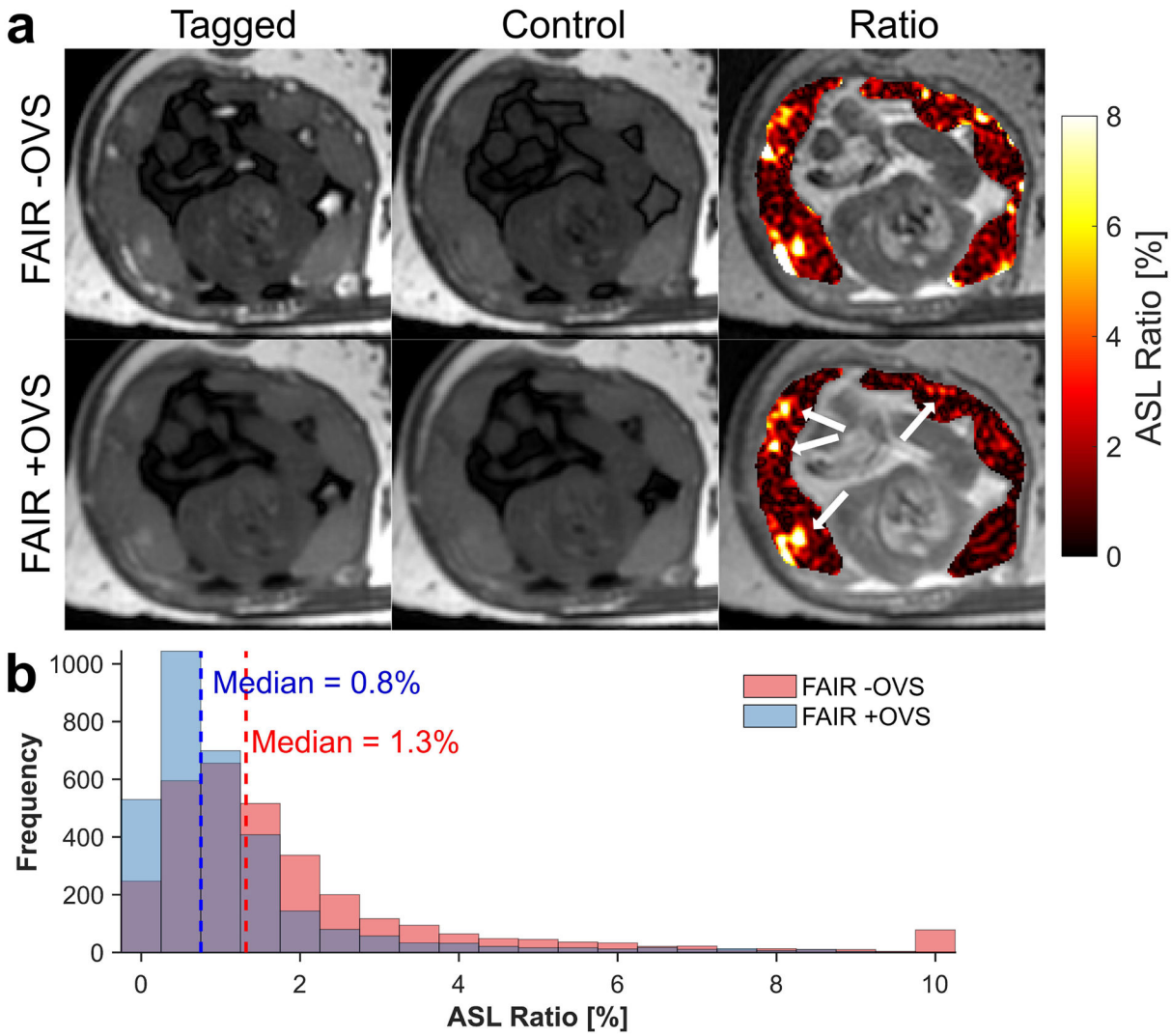

FIG. 3.

Representative ASL FAIR images (**a**, top row) show the FAIR tagged (left column), control (center column), and the perfusion ratio percentage map (right column), shown in color scale, overlaid on a proton density weighted image, shown in gray scale. OVS pulses were added to the ASL FAIR after FAIR tagging (**a**, bottom row) to reduce macrovascular signal on the periphery of placental tissue. Several localized perfusion regions within the placenta remain in the +OVS ratio map and these regions are highlighted by the white arrows. A histogram plot of the ASL ratio percentage (**b**) within the placental tissue for both ASL acquisitions is shown for one case ($N = 1$).

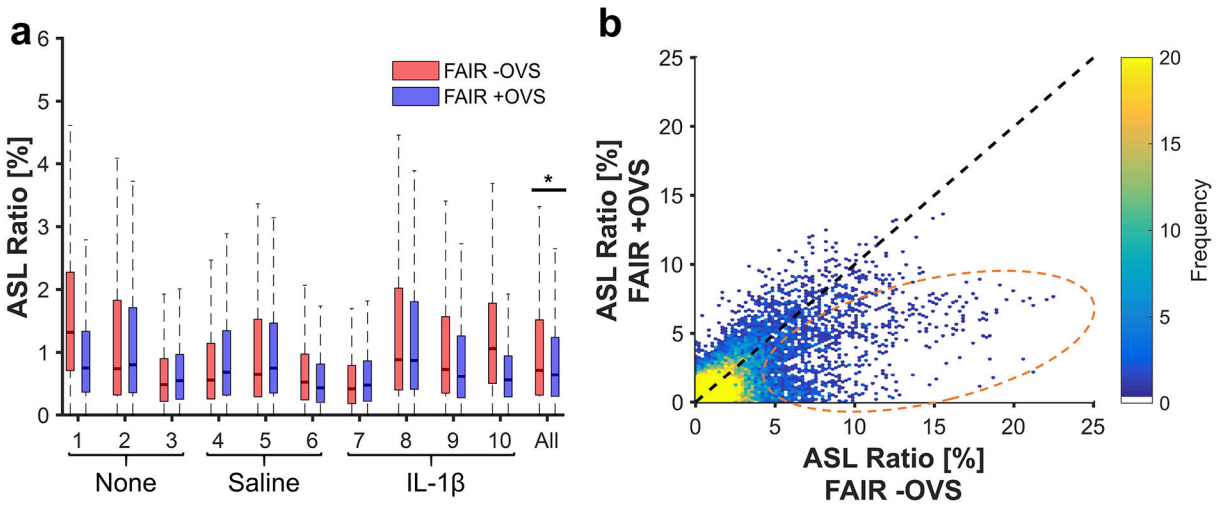

FIG. 4.

A comparison between the distributions of the ASL ratio percentages within the placental tissue for each individual macaques and for all macaques grouped together is shown as a box-and-whisker plot (**a**) for the two ASL FAIR pulse sequences: with (+OVS) or without (-OVS) the addition of OVS RF pulses. A voxel-wise density plot (**b**) of the ASL FAIR ratio percentage for corresponding spatial locations in either the +OVS or –OVS variant. The region with voxels having reduced ASL ratio with addition of OVS pulses are circled. An identity line (black-dotted line) is also plotted for reference.

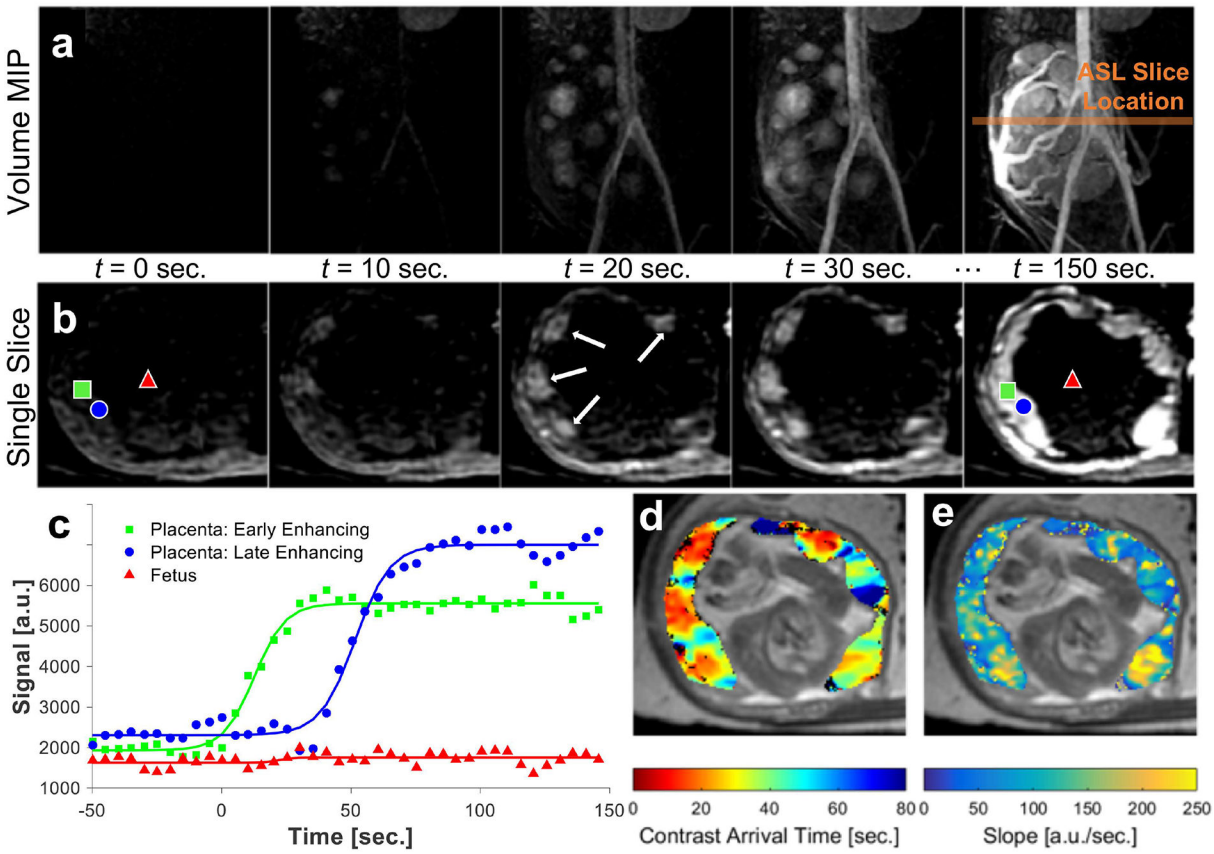

FIG. 5.

Dynamic contrast enhanced (DCE) MR images acquired throughout the injection of ferumoxytol. Maximum intensity projection (MIP) images (**a**) of the whole placenta and major vessels from a T_1-weighted DCE time series shown at 10 second time frames. The location of the ASL slices (orange line) is denote on the MIPs. The corresponding axial slice (**b**), matching the location of the ASL slice, is shown at corresponding time frames. Regions of early contrast arrival are highlighted (white arrows). The DCE signal enhancement and sigmoid curve fits (**c**) are shown for single voxels in two locations within the placenta, early (■) and late enhancing (●), and for a single voxel within the fetus (▲). The voxel locations are also highlighted in the final DCE time series image. Parameter maps derived from the fitted DCE data show the contrast arrival time (**d**) and the estimated relative blood flow (**e**) to the placental tissue. Parameter maps are shown (color scale) overlaid on an anatomical reference image (gray scale).

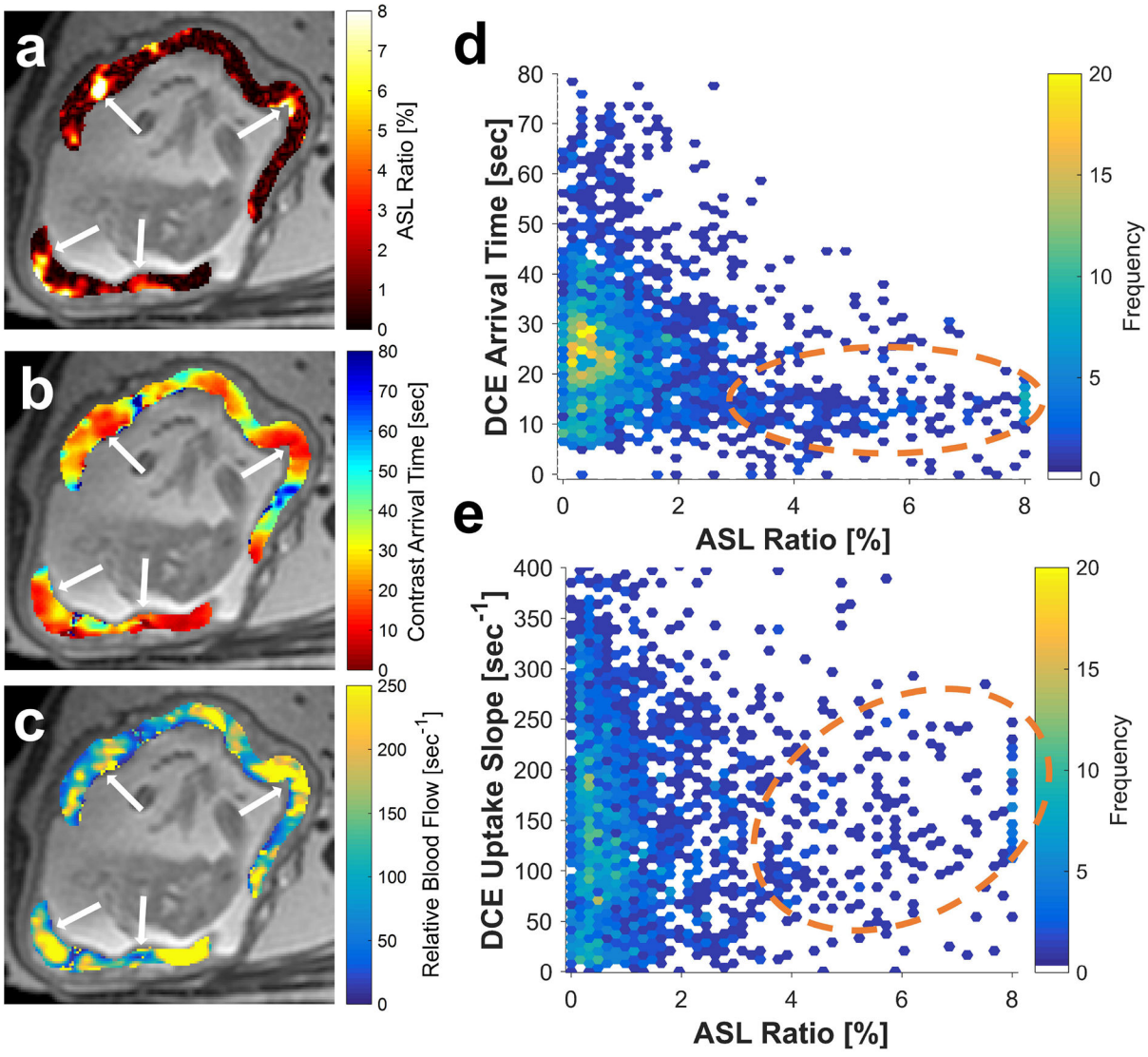

FIG. 6.

A regional comparison between the parametric maps of perfusion: ASL (FAIR +OVS) ratio (**a**), DCE contrast arrival times (**b**), and DCE relative blood flow (**c**) within the placental tissue. Spatial similarities between voxels with high ASL ratio percentage, early contrast arrival, and high relative blood flow are indicated by the white arrows. The parameter maps are shown in color scale overlaid on an anatomical reference image in gray scale. A voxel-wise density plot (**d**) between ASL ratio and uptake slope is shown for a representative case (N=1). The region with voxels having both high ASL ratio and early contrast arrival times is circled. A second voxel-wise density plot (**e**) between ASL ratio and uptake slope shows a circled region with a slight association between voxels with high ASL ratio coinciding with voxels with high uptake slope.

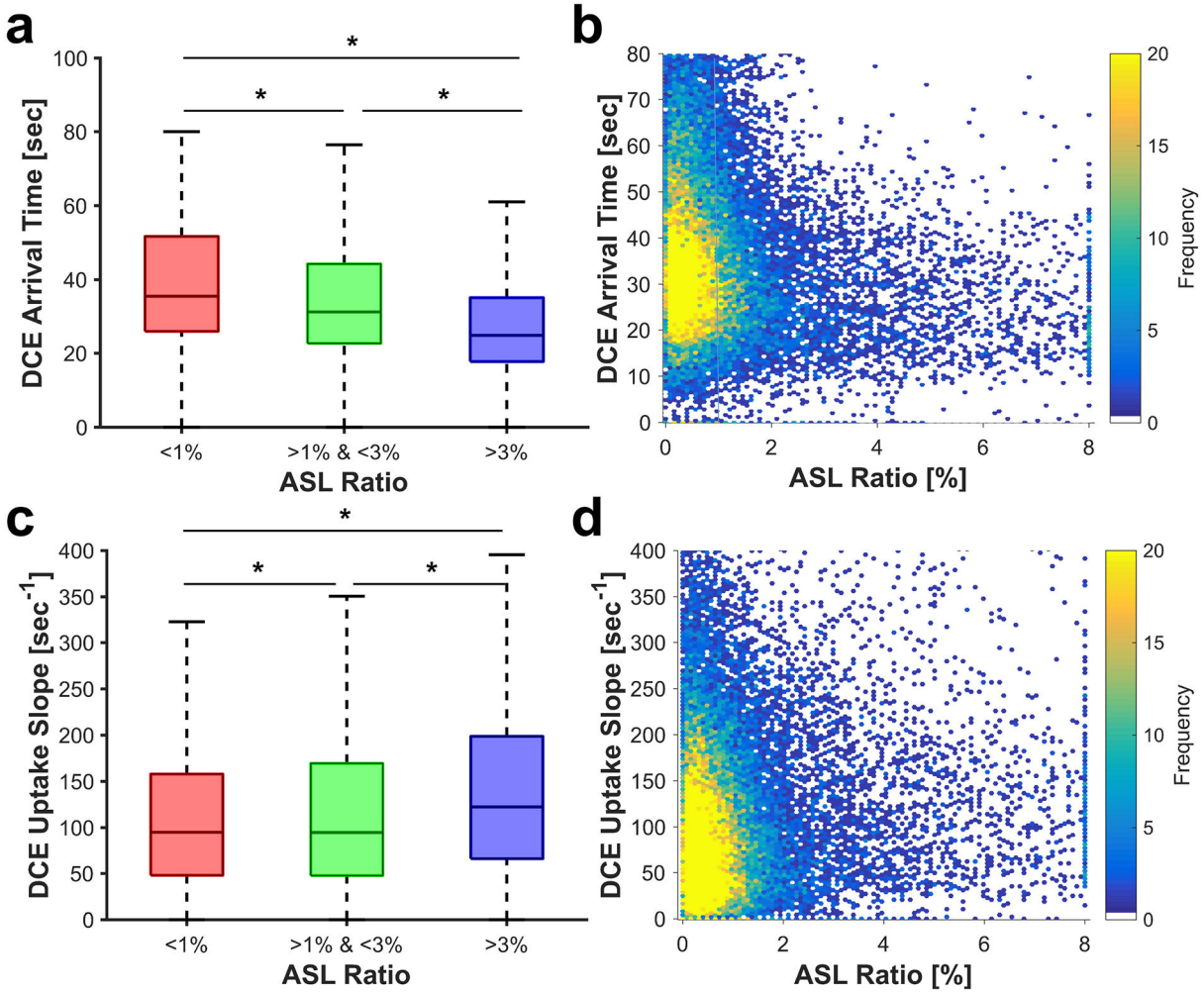

FIG. 7.

Box-and-whisker plots (**a**) comparing the ASL ratio percentage versus either the DCE contrast arrival time or the DCE uptake slope (**b**) for all macaques ($N = 10$). A Wilcoxon rank-sum test shows statistically significant differences between the three groups. The voxel-wise density plots are shown for the ASL ratio percentage versus either the DCE arrival time (**c**) or the DCE uptake slope (**d**). (* = $p < 0.05$)

Table 1.

Summary of animal characteristics in this study (*N*=10). All animals were in late 2nd trimester based on an average 166-day gestational period for the rhesus macaque. The mean ± SD of the gestational age and maternal weight is shown for all animals grouped together.

Animal Number	Intervention	Gestational Age [days]	Maternal Weight [kg]
1	None	91	9.90
2		99	10.02
3		106	10.04
4	Saline	98	8.56
5		100	9.06
6		104	7.09
7	IL-1β	93	8.56
8		93	9.77
9		99	7.63
10		109	8.65
All (*N*=10)		99.2 ± 5.9	8.93 ± 1.03

Table 2.

Summary of the ASL perfusion measurements within the rhesus macaque placenta for the three subgroups. The median ± SD and quartile values [5% and 95%] from the ASL ratio percentage for both FAIR acquisitions are tabulated.

	ASL Ratio [%]			
	FAIR −OVS		FAIR +OVS	
Intervention	**Median ± SD**	**Quartiles [5 – 95%]**	**Median ± SD**	**Quartiles [5 – 95%]**
None (*N*=3)	0.81 ± 2.37	[0.07 – 6.11]	0.69 ± 1.47	[0.06 – 4.07]
Saline (*N*=3)	0.57 ± 1.83	[0.05 – 4.93]	0.61 ± 1.56	[0.06 – 4.71]
IL-1β (*N*=4)	0.75 ± 1.73	[0.06 – 4.62]	0.62 ± 1.26	[0.06 – 3.45]
All (*N*=10)	0.71 ± 2.00	[0.06 – 5.21]	0.64 ± 1.42	[0.06 – 4.01]

Table 3.

Summary of the ferumoxytol DCE measurements of the contrast arrival time and relative blood flow within the rhesus macaque placenta for the three interventions. The median ± SD and quartile values [5% and 95%] for the DCE parameters are tabulated.

	DCE Parameter			
	Contrast Arrival Time [sec]		Relative Blood Flow [sec^{-1}]	
Intervention	**Median ± SD**	**Quartiles [5 – 95%]**	**Median ± SD**	**Quartiles [5 – 95%]**
None (*N*=3)	33 ± 31	[11 – 107]	112 ± 34	[21 – 288]
Saline (*N*=3)	35 ± 21	[16 – 76]	85 ± 34	[17 – 252]
IL-1β (*N*=4)	33 ± 23	[16 – 72]	106 ± 50	[15 – 388]
All (*N*=10)	34 ± 25	[14 – 87]	102 ± 39	[17 – 336]